Fermi surface as a driver for the shape-memory effect in AuZn

2005 J. Phys.: Condens. Matter 17 L69

(http://iopscience.iop.org/0953-8984/17/6/L01)

INSTITUTE OF PHYSICS PUBLISHING JOURNAL OF PHYSICS: CONDENSED MATTER

J. Phys.: Condens. Matter **17** (2005) L69–L75 doi:10.1088/0953-8984/17/6/L01

LETTER TO THE EDITOR

Fermi surface as a driver for the shape-memory effect in AuZn

R D McDonald[1], J Singleton[1], P A Goddard[1], F Drymiotis[1], N Harrison[1], H Harima[2,3], M-T Suzuki[2,3], A Saxena[1], T Darling[1], A Migliori[1], J L Smith[1] and J C Lashley[1,4]

[1] Los Alamos National Laboratory, Los Alamos, NM 87545, USA
[2] ISIR Osaka University, Ibaraki, Osaka 567-0047, Japan
[3] Department of Physics, Kobe University, 1-1 Rokko-dai Noda, Kobe 657-8501, Japan

E-mail: rmcd@lanl.gov

Received 24 December 2004
Published 28 January 2005
Online at stacks.iop.org/JPhysCM/17/L69

Abstract

Martensites are materials that undergo diffusionless, solid-state transitions. The martensitic transition yields properties that depend on the history of the material and may allow it to recover its previous shape after plastic deformation. This is known as the shape-memory effect (SME). We have succeeded in identifying the primary electronic mechanism responsible for the martensitic transition in the shape-memory alloy AuZn by using Fermi-surface measurements (de Haas–van Alphen oscillations) and band-structure calculations. This strongly suggests that electronic band structure is an important consideration in the design of future SME alloys.

The martensitic transition (MT) is widely encountered in nature, with examples being observed in cuprate superconductors [1], polymers [2], transition metal alloys [3] and actinides [4]. A subclass of these materials exhibit the shape-memory effect (SME) where, following deformation of the low-temperature martensitic phase, they recover their high-temperature shape on warming through the transformation [5]. One practical example of this phenomenon is the use of nitinol (NiTi alloys) for stent implants used to increase flow in restricted blood vessels. Before insertion the stent is compressed and expands the vessel after warming to human body temperature [6].

In elemental metals and simple metallic alloys, the band electrons act as the quantum-mechanical 'glue' that binds the atoms in a particular structural arrangement [7]; hence, these electrons are likely to be of great importance in spontaneous structural rearrangements such as the MT. Indeed, in several other classes of material, instabilities amongst the band electrons are

[4] Author to whom any correspondence should be addressed: e-mail j.lash@lanl.gov

already known to be responsible for structural phase transitions (see e.g., [4, 8]). In spite of this fact, and notwithstanding the importance of SME alloys in medicine and technology, very few opportunities have existed for experiments that elucidate directly the relationship between band electrons and the MT [9]. To address this question, we have prepared a stoichiometric (disorder-free) SME alloy, AuZn, that shows a MT at 64 K, and made the first detailed measurements of its Fermi surface, the constant-energy surface in wavevector space that defines the band-electron dynamics. By comparing the data with the first band-structure calculations of a martensite of this complexity (18 atoms per primitive unit cell with no inversion symmetry) we are able to ascertain the role of band electrons in the SME. This is an important step towards the design of future SME alloys with greater recoverable strain and improved functionality; because the high-temperature austentite, or parent, phase of AuZn shares the same B2 cubic symmetry as the more familiar NiTi [10] and AuCd [11] SME alloys, it constitutes a paradigm for understanding the mechanism of this important effect.

Despite the similarities between AuZn and other SME alloys, the fact that its MT is only accessible using cryogens has made it much less studied. However, it is exactly this low-temperature transition that makes AuZn ideal for a study assessing the fundamental role of the electrons; in higher temperature martensites that role is often confused by the entropic contribution from the phonons.

The transition takes place as follows [12, 13]: as the temperature is lowered through the MT, the unit cell is distorted in the [110] shear direction. A strain and commensurate shuffle of every third unit cell results in a hexagonal primitive unit cell formed from nine primitive cubic cells of the parent phase. This structure can also be described in terms of its conventional rhombohedral unit cell; however, we limit our discussion to the primitive hexagonal unit cell as this is most informative when considering the relationship between the Brillouin zone (the unit cell in wavevector space) and a real-space distortion.

Our single-crystal samples of AuZn were prepared by the method outlined in [14]. Resistivity data were acquired using the standard four-terminal technique at temperatures down to 500 mK in either a 33 T Bitter magnet or a 17 T superconducting magnet. Heat capacities were collected using a Quantum Design PPMS employing a thermal relaxation method. The excess heat capacity (i.e. that with the conventional phonon and electronic components subtracted) was computed in [14]. Magnetization measurements employed a capacitative torque magnetometer on a two-axis cryogenic goniometer, allowing samples to be rotated to all angles in the magnetic field without thermal cycling. Three planes of rotation intersecting symmetry directions of the parent phase were used, field sweeps being recorded every 3°. The initial sample orientation was determined by a Laue camera.

Figure 1(A) shows the excess heat capacity for three single crystals of AuZn covering the range of composition exhibiting the SME. The transition from the high-temperature austenite to low-temperature martensite is clearly visible as a single peak in the excess heat capacity at temperatures of 90 K ($Au_{0.47}Zn_{0.53}$), 67 K (AuZn) and 40 K ($Au_{0.52}Zn_{0.48}$), confirming that this alloy has the lowest-temperature shape-memory transition yet measured. Formation of martensite produces a vibrational entropy associated with the structural change along with a contribution from the number of distinct orientations that the variants can assume with respect to the parent phase [15, 16]. The absence of other features besides this peak is clear evidence that there are no precursor phases and that there is a simple atomic path through the transformation. Cryogenic deformation was used to demonstrate that the SME occurs in AuZn [14].

A very significant change in magnetoresistance of AuZn at the MT is observed (figures 1(B), (C)). In non-magnetic metals, magnetoresistance is caused by field-induced motion of electrons across the Fermi surface, resulting in an alteration of the time-dependent evolution of their velocities [7]. In the absence of magnetic order, the large change in

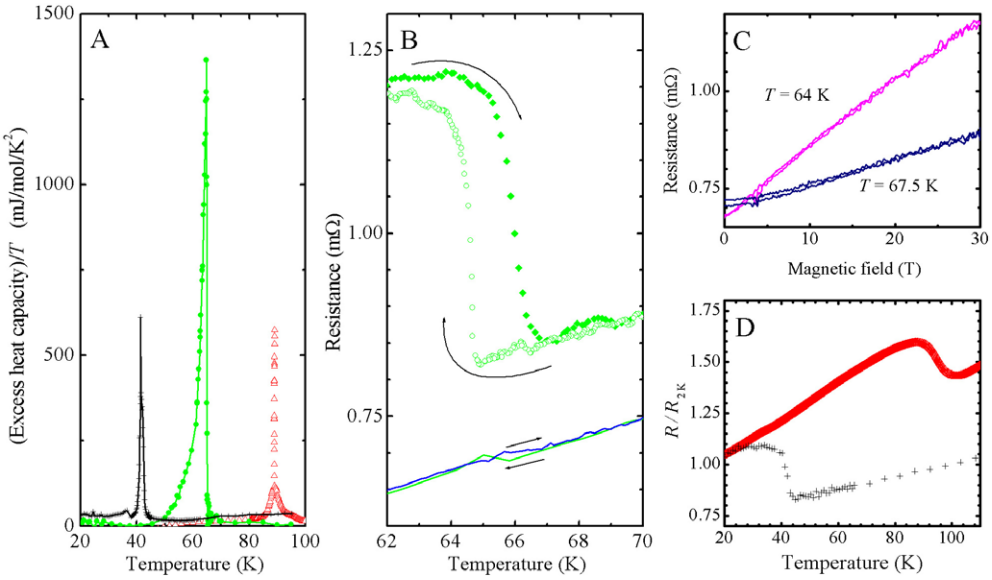

Figure 1. (A) Excess heat capacity (i.e. experimental heat capacity minus the slowly varying background phonon contributions (11)) of $Au_{0.52}Zn_{0.48}$ (crosses), AuZn (filled circles) and $Au_{0.47}Zn_{0.53}$ (triangles). (B) Resistance of AuZn at zero magnetic field (curves) and at 25 T (points) versus temperature. In both cases, data for cooling and warming are shown. (C) Magnetoresistance of AuZn at 67.5 K (blue curves) and at 64 K (steeper red curves); data for both rising and falling field are shown. (D) Resistance (normalized to the value at 2 K) of $Au_{0.52}Zn_{0.48}$ (crosses) and $Au_{0.47}Zn_{0.53}$ (triangles) samples versus temperature (measured on cooling). Note how the zero-field resistance of the off-stoichiometric alloys exhibits a large step at the MT (D), whereas the resistivity of the equiatomic alloy (B) only develops a large step in magnetic field.

magnetoresistance at the MT can only indicate one thing, a marked modification of the Fermi surface [7, 8]. The effect that any such modification has on the temperature-dependent resistivity can be quite small, depending as it does on the details of the density of states at the Fermi energy and the quasiparticle effective masses on either side of the transition. By contrast, the magnetoresistance is affected primarily by the shape of the electronic orbits and hence is a sensitive gauge of changes in Fermi-surface topology. This change in magnetoresistance, plus the large value (typically ∼30–40) of the ratio of the sample resistance at 300 K to that at 4.2 K and the low temperature of the martensite transition, suggest that a study of the Fermi-surface topology of AuZn would be informative, feasible and contain all of the essential physics. Hence the martensite phase was studied using the de Haas–van Alphen effect.

In the de Haas–van Alphen effect, the frequencies, F (in tesla), of the magnetic quantum oscillations are proportional to extremal cross-sectional areas of the Fermi surface in the planes perpendicular to the magnetic field [7]. The oscillations can be directly related to the electronic density of states and Fermi–Dirac distribution function [7]. Typical raw de Haas–van Alphen data are shown in figure 2(A). The oscillations become visible at a field of around $B_0 \sim 1.5$ T, suggesting that the electrons have a relatively long mean free path, λ. Using the approximation $\lambda \sim (hF/\pi e)^{1/2}/B_0$, where h is Planck's constant and e is the electronic charge [7], we obtain $\lambda \sim 0.2\ \mu$m. Such long mean free paths, comparable to those in the best binary alloys [17], imply that our $Au_{0.50}Zn_{0.50}$ samples are exceptionally free of impurities and defects. Therefore the SME is an intrinsic property of pure AuZn.

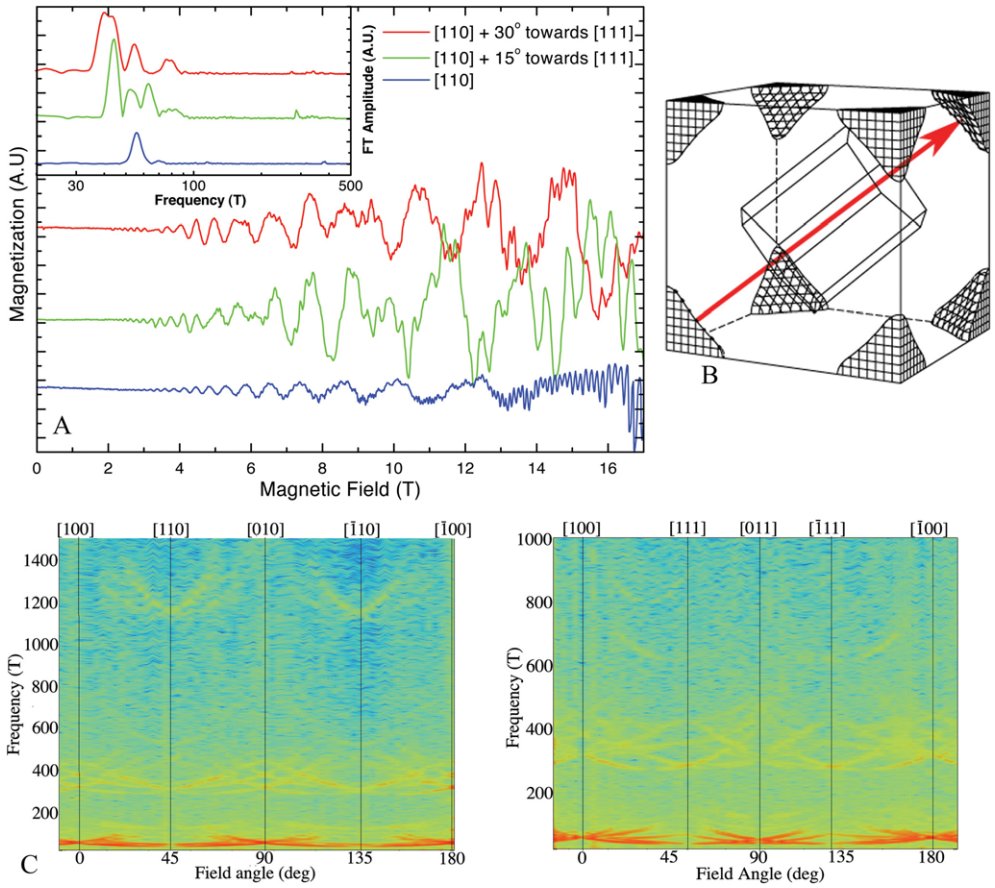

Figure 2. (A) de Haas–van Alphen oscillations of a AuZn single crystal at a temperature of 0.75 K plotted as magnetization versus magnetic field for three different field angles. The inset contains Fourier transforms of the same data. (B) The hexagonal martensite-phase Brillouin zone enclosed within the cubic austenite Brillouin zone; the 14th band (hole) Fermi surface of the austenite is also shown, as is the proposed nesting vector (red arrow). The equivalence of the four possible orientations of the hexagon along the body diagonals of the cube is responsible for both the shape-memory effect associated with the transition and the cubic symmetry of the data in (C). (C) de Haas–van Alphen spectra plotted as Fourier amplitude (colour scale—red is high intensity, blue is background) versus frequency and field angle for rotations of the sample in 3° steps about the austenite [001] direction (left) and [01$\bar{1}$] direction (right).

The inset to figure 2(A) shows Fourier transforms of typical data. As expected in a system with a large unit cell resulting from a complex shuffle, there is a plethora of low frequencies indicating a Fermi surface comprising many small pockets. To investigate further the Fermi-surface topology, magnetization data were recorded for many orientations of the sample in the field. Owing to the low symmetry of the martensite phase (figure 2(B)) three separate axes of rotation were chosen. Rotations of 180° about each axis were used to allow the magnetic field to lie along a number of symmetry directions of the austenite phase. Figure 2(C) shows a mapping of the Fourier amplitudes of the various de Haas–van Alphen frequencies, each corresponding to a particular Fermi-surface cross-section. The frequencies show a very well defined angular periodicity with several frequencies converging when the field is applied along

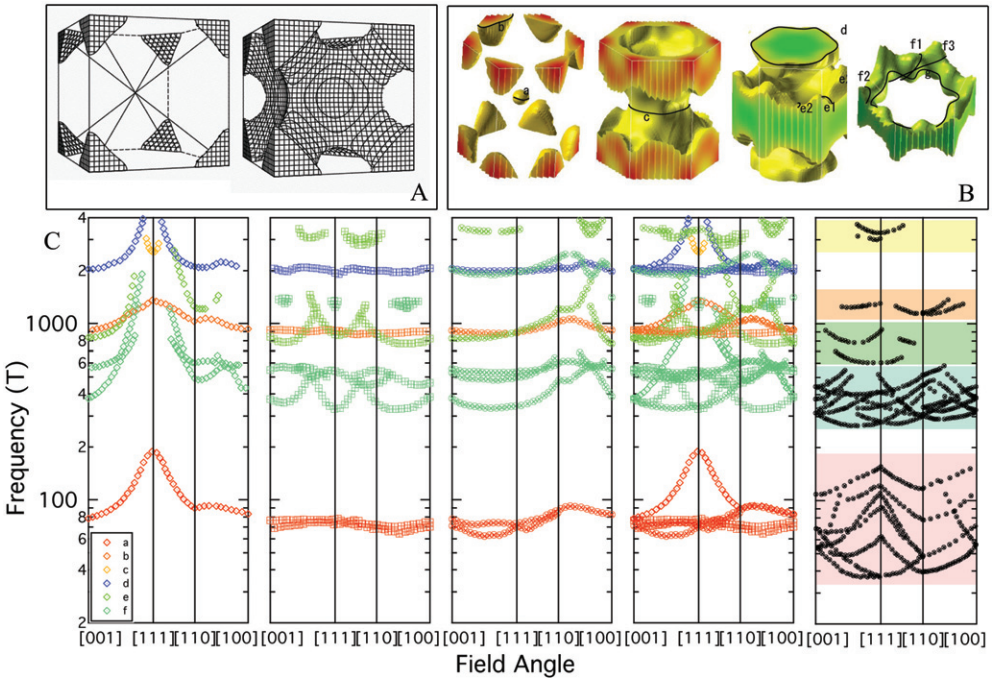

Figure 3. (A) The calculated Fermi surfaces for the austenite phase of equiatomic AuZn (left, 14th band; right, 15th band). (B) The calculated Fermi surfaces for the martensite phase; the small letters label the Fermi surface orbits that give rise to various de Haas–van Alphen oscillations. (C) The three left-hand figures show de Haas–van Alphen frequencies as a function of field angle (with respect to the austenite-phase axes) predicted by the band-structure calculations for equiatomic AuZn in the martensite phase. From left to right, the plots are for the martensite domain with the *c*-axis oriented along the austenite [111] direction, those along the $[1\bar{1}1]$ and $[\bar{1}11]$ directions and that along the $[11\bar{1}]$ direction respectively. The fourth plot is the sum of all domain orientations. The right-hand plot shows the observed de Haas–van Alphen frequencies as a function of field angle (again with respect to the austenite-phase axes). The coloured bands are a guide to the eye, linking the observed frequencies with those predicted. Labels a–f indicate the Fermi-surface orbits responsible for each frequency (see (B)).

the parent-phase symmetry directions. This observation demonstrates that there is a single-variant, low-temperature phase and that domains corresponding to all four possible orientations of the hexagonal distortion are present in roughly equal numbers, each possessing a well defined angular relationship with each other and with the parent phase (figure 2(B)). The mean free path of $\sim$0.2 μm, inferred from the de Haas–van Alphen effect, represents an order-of-magnitude estimate for the linear dimensions of the domains.

In order to understand better the Fermi-surface topology, band-structure calculations were performed for the austenite and martensite phases. Atomic positions in the martensite phase were based on established group-theoretical arguments [13]. For the martensite phase the calculations are performed on the primitive hexagonal unit cell, containing nine AuZn pairs [13]. The calculations include the effects of spin–orbit interactions by means of a full-potential linear augmented-plane-wave (FLAPW) method [17]. The exchange–correlation potential was modelled by means of a local-density approximation (LDA).

Figure 3 shows the calculated Fermi-surface sections of the martensite phase (figure 3(B)) along with their predicted de Haas–van Alphen frequencies as a function of field orientation

(figure 3(C)). Note that three separate field-orientation dependences are shown to account for the four possible orientations of the martensite distortion. Theoretical frequencies from these orientations are compared with those observed in the experiments on the far right-hand side of figure 3(C). The observed frequencies fall into the ranges encompassed by the predictions, and many of their angular dependences are reproduced qualitatively.

The success of the band-structure calculations enables us to suggest the way in which the Fermi-surface modification is associated with the MT. In the austenite phase, two bands cross the Fermi energy, producing two Fermi-surface sheets (figures 2(B), 3(A)). The sheet originating from the 14th band has approximately planar faces orthogonal to the cubic $\langle 111 \rangle$ directions. Opposed planar faces of this type make a metal prone to a spontaneous distortion [7, 8]. If a single 'nesting vector' (shown as a red arrow in figure 2(B)) can map a large area of Fermi surface onto its symmetry-related equivalent, the electronic system can reduce its energy by opening a gap across those Fermi-surface sheets [8]. In real space, the nesting reveals itself as a spatial modulation of the electronic density and may be accompanied by a periodic distortion of the lattice via electron–phonon coupling. Such transitions occur provided the elastic energy cost of distorting the crystal to encompass the new periodicity, represented by the nesting vector, is outweighed by the energy saved by gapping the electronic system [8]. Systems with purely one-dimensional Fermi surfaces always exhibit this instability, and the resulting distortion is known as the Peierls distortion [7, 8]. In the case of AuZn's austenite phase, there are four equivalent proposed nesting vectors corresponding to the four body diagonals of the cubic Brillouin zone. This explains the four crystallographically-related domains found in the martensite phase (figure 2(B)).

In a low-symmetry metal with a one-dimensional Fermi surface, a Peierls distortion can be either commensurate with the lattice if the Fermi momentum is a rational fraction of the momentum at the Brillouin-zone boundary, or incommensurate if it is not [8]. In either case, to first order, the lattice distortion moves successive planes alternately closer together and further apart, thus introducing a new periodicity without changing the sample length. In a high-symmetry metal with multiple planar Fermi-surface sheets the situation may be different. If the separation of the planar sections of the Fermi surface is not a rational fraction of a dimension of the Brillouin zone, a crystallographic distortion resulting in a net length change along the preferred direction can change the relative Fermi- and Brillouin-zone momenta (this cannot occur in a one-dimensional metal), facilitating a commensurate distortion that gaps the Fermi-surface sheet in question. A commensurate distortion is preferred because the reduction in electronic energy is greater than for the incommensurate case. This is precisely the situation that measurements indicate for the MT in AuZn, thus providing an explanation for the SME: in AuZn, the momentum of the 14th band Fermi surface is close to, but not exactly, two-thirds of that of the Brillouin-zone boundary such that the distortion must not only triple the unit cell to gap these Fermi-surface sections but also change the length of the sample in that direction so as make the distortion commensurate. It is the net length change of one of the sample dimensions relative to the others that gives AuZn its SME properties, enabling it to strain in response to an applied stress by changing the relative number of domains oriented in each direction. The strain is hence recoverable upon warming through the MT, and AuZn exhibits the SME. The experiments and calculations reported here have not only brought this mechanism to light, but strongly suggest important considerations for the design of future SME alloys; i.e., the ideal requirements for the austenite phase are near-planar Fermi-surface sections linked by geometrically-degenerate nesting vectors that are close to commensurate with the Brillouin zone.

This electronic mechanism may also explain the trend in MT temperature with composition (figure 1(A)). Zinc contributes two electrons to the filling of the upper bands in

AuZn, whereas gold only contributes one. As the band filling increases with zinc composition, the size of the hole Fermi-surface pockets in the austenite phase will shrink slightly. More importantly, they will 'flatten out', so that a distortion will be able to gap a greater fraction of states at the Fermi energy. This will increase the amount of free energy gained and raise the transition temperature.

In summary, magnetoresistance data show that the martensitic transformation in AuZn is associated with a single, distinct rearrangement of the Fermi surface. In combination with heat-capacity experiments, this demonstrates that the transformation is free of the complications of precursor phases. Furthermore, the low transition temperatures imply that effects due to diffusion [18] and vibrational entropy can be ruled out. The de Haas–van Alphen data suggest an order-of-magnitude length scale for the martensite domains and are in agreement with band structure calculations. Most importantly, the data and calculations provide direct evidence about the role of the band-electron system and its Fermi surface in the SME. This indicates that band-structure/property relations are an important consideration for the design of future SME alloys.

This work is supported by the United States Department of Energy (DoE) Primary Physics Experimental Program and by DoE grant No LDRD-DR 20030084. Part of this work was carried out at the National High Magnetic Field Laboratory, which is supported by the National Science Foundation, the State of Florida and DOE. We thank M Ahlers, T Lookman, and D Lieberman for many informative sessions. We also thank Luis Balicas and Ali Bangura for experimental assistance.

References

[1] Lavrov A N, Komiya S and Ando Y 2002 *Nature* **418** 385–6
[2] Anseth K S and Burdick J A 2002 *Mater. Res. Soc. Bull.* **27** 130–6
[3] Bhattacharya K, Conti S, Zanzotto G and Zimmer J 2004 *Nature* **428** 55–9
[4] Lander G H, Fisher E S and Bader S D 1994 *Adv. Phys.* **43** 1–11
[5] Schmerling M A and Karz R W 1975 *Shape Memory Effects in Alloys* (New York: Plenum)
[6] Duerig P W 2002 *Mater. Res. Soc. Bull.* **27** 101
[7] Abrikosov A A 1988 *Fundamentals of the Theory of Metals* (Amsterdam: North-Holland)
[8] Grüner G 1994 *Density Waves in Solids* (Boston: Addison-Wesley)
[9] Ahlers M 1996 *Z. Phys.* B **99** 491–9
[10] Wayman C M and Shimizu K 1972 *Met. Sci. J.* **6** 175
[11] Wechsler M S and Read T A 1955 *J. Appl. Phys.* **26** 473
[12] Makita T *et al* 1995 *Physica* B **213/214** 430–2
[13] Barsch G R 2000 *Mater. Sci. Forum* **327/328** 367–76
[14] Darling T W *et al* 2002 *Phil. Mag.* B **82** 825–37
[15] Pops H and Massalski T B 1965 *Trans. AIME* **233** 728
[16] Romero R and Pelegrina J L 2003 *Mater. Sci. Eng.* A **354** 243
[17] Harrison N *et al* 2000 *Phys. Rev.* B **61** 1779–85
[18] Gupta D and Lieberman D S 1971 *Phys. Rev.* B **4** 1070–8